A CONSISTENT DESIGN PROCEDURE FOR SUPERCRITICAL AIRFOILS IN FREE AIR AND A WIND TUNNEL*

Vijaya Shankar and Norman D. Malmuth
Rockwell International Science Center

Julian D. Cole
University of California, Los Angeles

SUMMARY

A computational inverse procedure for transonic airfoils in which shapes are determined supporting prescribed pressure distributions is presented. The method uses the small disturbance equation and a consistent analysis-design differencing procedure at the airfoil surface. This avoids the intermediate analysis-design-analysis iterations. The effect of any openness at the trailing edge is taken into account by adding an effective source term in the far field. The final results from a systematic expansion procedure which models the far field for solid, ideal slotted and free jet tunnel walls are presented along with some design results for the associated boundary conditions and those for a free flight.

INTRODUCTION

Computational design or inverse procedures for transonic airfoils in which shapes are determined supporting prescribed pressure distributions have been in use since the early work of Nieuwland[1]** which employed hodograph methods to calculate shock-free supercritical flow about a family of quasi-elliptical airfoils. Later Garabedian and Korn[2] developed a more general hodograph procedure to design highly cambered shock-free airfoils. In spite of their usefulness, hodograph procedures for design purposes have several disadvantages. They require too many input parameters, are restricted to shock-free solutions, and are not easily extendable to design of three-dimensional wings. Steger and Klineberg[3] treated the problem within a small-disturbance framework solving the continuity and vorticity equation at interior points. To insure consistency between the analysis and the design formulation, they applied appropriate discretization procedures to the vorticity equation at the airfoil grid points. However, the first-order system with velocity components as dependent variables produces a difficulty in the treatment of singularities at the airfoil nose and trailing edge. The effect of nose and trailing edge singularities could be greatly reduced by

*Part of the work was presented at the AIAA 16th Aerospace Sciences Meeting, Paper No. 78-103. A portion of this effort was sponsored by the Air Force Office of Scientific Research under U.S. Air Force Contract No. F44620-76-C-0044.

**Reference citation is given by numerical superscript.

using a scalar formulation involving the velocity potential. Tranen[4] employed the full potential equation to remedy the deficiency inherent in the small disturbance formulation at the leading and trailing edges. To overcome the inaccuracies and inconsistencies in his formulation associated with the discretization procedures at the boundary, iterations must be employed between direct and inverse solvers. Also, in the full potential formulation, boundary conditions are to be applied at the exact airfoil surface. Since the airfoil surface is unknown in the design problem, errors propagate due to application of boundary conditions at some assumed airfoil surface. Carlson[5] used ghost point and higher order accurate methods to handle airfoil boundary points. Rather than employing the circle plane as in Tranen's procedure, Carlson used a Cartesian framework. However, even his procedure is not consistent in the sense that the discretizations used for C_p in the analysis and those in the design phase are not of the same form. The former uses a central differenced ϕ_x for C_p calculations while the latter employs a special backward differenced ϕ_x involving ghost points. As a result, perfect agreement between his analysis and design calculations is not to be expected, especially near the shock. Also, the problems associated with open trailing edges are not addressed in his work. The trailing edge is made to close by altering the nose shape. However, in his intermediate calculations, large open trailing edges occur. The final results are questionable since the effect of openness is not included in the far field for the intermediate solutions.

In this paper, a small-disturbance model employing the velocity potential as the dependent variable is used for the implementation of the design algorithm. This procedure simplifies the treatment of boundary conditions and alleviates the need for mappings that arise in a full potential equation formulation. A mixed boundary value problem is solved in which Neumann data are specified in the first few percent of the chord length where the assumed shape is retained, and Dirichlet conditions are prescribed on the rest of the airfoil where the pressure is to be modified. One important thrust of the present work is in developing a consistent discretization procedure for the airfoil grid points. If the converged C_p output from the analysis is not altered, then the design mode recovers the same airfoil shape without any discontinuity in the airfoil slope at the shock wave, overcoming a deficiency in Carlson's work. Another significant feature of the numerical implementation not considered by the previous investigators is the effect of an open trailing edge in the far field. In the present work, this is accounted for with the addition of the necessary source terms in the far field. Design of thick trailing edge airfoils is of interest in inviscid flow to achieve a reasonable trailing edge thickness after accounting for the viscous displacement thickness. Some amount of trailing edge thickness is required from a structural stability point of view. Figure 1 schematically explains the design philosophy followed in this paper. The top of Figure 1 shows a conventional airfoil at transonic speed producing a shock on the upper surface. Specifying a shockless pressure distribution on the upper surface would flatten the upper surface of the conventional airfoil, thereby producing an openness at the trailing edge. This is shown in the middle of Figure 1. The amount of trailing edge openness can be reduced by specifying a lower surface pressure distribution with a large aft end loading. This kind of loading undercuts the lower surface producing a Whitcomb[6] type supercritical airfoil.

A typical supercritical airfoil design is presented in the Results section. The effects of wind tunnel walls in the computation of transonic airfoil design and analysis have also been studied. The downstream and upstream infinity conditions for the solid, ideal slotted, and free jet tunnel walls have been derived from a systematic asymptotic solution of the small-disturbance integrodifferential equation.

SYMBOLS

$\vec{B}$	scaled mass flux vector
C	chord
C_L	lift coefficient
c_n	section normal-force coefficient
$C_p\Big\|_{i-1/2,j}$	pressure coefficient at half node points
$F'_{u,\ell}$	upper and lower airfoil slopes
H	scaled half tunnel wall height
K	transonic similarity parameter
M	Mach number
M_∞	free stream Mach number
Q	effective source strength due to airfoil trailing edge openness
$x,\tilde{y}$	coordinate system
$y_{u,\ell}$	upper and lower airfoil ordinates
ϕ	velocity potential
ϕ_{FF}	far field velocity potential
α	angle of attack
δ	maximum airfoil thickness
γ	specific heat ratio

EQUATION AND BOUNDARY CONDITIONS

The transonic small disturbance equations are formally derived by an asymptotic expansion procedure[7] applied to the Euler equations. For an airfoil whose upper and lower surfaces are defined by $y_{u,\ell} = \delta F_{u,\ell}(x) - \alpha x$ the perturbation potential satisfies the equation

$$[K - (\gamma+1)\phi_x]\phi_{xx} + \phi_{\bar{y}\bar{y}} = 0 \tag{1}$$

The large lateral propagation of transonic disturbances is taken into account by the use of the scaled coordinate $\bar{y} = y\delta^{1/3}M_\infty^{2/3}$. The limit process is $\delta \to 0$, $M_\infty \to 1$, while x,y, and $K = (1-M_\infty^2)/(M_\infty\delta^{2/3})$ remain fixed. The quantity α is the angle of attack.

Consistent with the small disturbance formulation, the airfoil boundary conditions are applied on a slit of $\bar{y} = 0$. In the case of pure analysis the airfoil boundary condition (flow tangency) is of Neumann type.

$$\phi_{\bar{y}}(x,0\pm) = F'_{u,\ell}(x) - \frac{\alpha}{\delta}, \qquad -1 \leqslant x \leqslant 1 \tag{2}$$

The airfoil leading and trailing edges are at $x = -1$ and $x = 1$ respectively. In the design problem, the airfoil shape corresponding to a given pressure distribution is sought. However, the small disturbance theory cannot resolve the nose region accurately. Therefore, the nose shape of an existing airfoil is specified for up to 5-10% of the chord length and a desired pressure distribution over the rest of the chord is prescribed. The boundary conditions then become a mixed Neumann-Dirichlet type. On the portion of the airfoil where the nose shape is specified, the boundary condition applied is given by Eq. (2). Over the rest of the airfoil a scaled pressure coefficient

$$C_p = -2\left(\delta^{2/3}/M_\infty^{3/4}\right)\phi_x(x,0\pm) \tag{3}$$

is prescribed. With $\phi_x(x,0\pm)$ known from Eq. (3), the perturbation potential $\phi(x,0\pm)$ is calculated by integration. This value of $\phi(x,0\pm)$ is then imposed at the airfoil slit as a Dirichlet type boundary condition. Figure 2 schematically illustrates the mixed Neumann-Dirichlet type boundary condition.

FAR FIELD

To avoid mapping procedures which bring infinity to a finite distance from the airfoil, but compromise the difference method, an approximate asymptotic solution for ϕ valid at large distances from the airfoil is used as far field

boundary condition. The type of far field depends on whether the airfoil is kept in free air or a solid, slotted or porous wall wind tunnel. The far field expressions to be used in this paper will now be discussed.

Free Air

Figure 2 shows the far field arrangement. Along the outer boundary ABCDE, the perturbation potential ϕ is computed from

$$\phi_{FF} = -\frac{\Gamma\theta}{2\pi} + \frac{Q\log\tilde{r}}{2\pi} + \ldots \tag{4}$$

where Γ is the circulation around the airfoil, $\theta = \tan^{-1}(\sqrt{K}\tilde{y}/x)$, Q is an effective source strength due to any openness at the trailing edge, and $\tilde{r} = \sqrt{x^2 + K\tilde{y}^2}$. Only dominant terms are kept in Eq. (4).

An expression for the source strength Q is obtained by considering the integral form of Eq. (1). The divergence theorem is used to obtain this integral relation in the cut region R shown in Figure 3

$$\iint_R \nabla\cdot\vec{B}\,dA = \oint_{C_1+C_2} \vec{B}\cdot\vec{n}\,ds \tag{5}$$

where $\vec{B} = (K\phi_x - \frac{(\gamma+1)}{2}\phi_x^2)\,\vec{i} + \phi_{\tilde{y}}\vec{j}$ is a scaled mass flux vector. Since $\vec{B}$ is is conserved across shock waves, no special boundary terms appear if shocks are present in the flow. Expanding Eq. (5) results in

$$\int_{-1}^{1} [\phi_{\tilde{y}}]dx = \int_{C_1} \left(K\phi_x - \frac{(\gamma+1)}{2}\phi_x^2\right)d\tilde{y} - \phi_{\tilde{y}}dx \tag{6}$$

Substituting Eq. (4) into Eq. (6) and simplifying gives

$$Q = \frac{1}{\sqrt{K}}\int_{-1}^{1} [\phi_{\tilde{y}}]dx, \text{ where } [\ ] \text{ denotes jump} \tag{7}$$

If the airfoil trailing edge is closed, then $\int_{-1}^{1} [\phi_{\tilde{y}}]\, dx$ is zero and no source term is present. While designing an airfoil to support a given pressure distribution the magnitude of the trailing edge openness is not known a priori. In the calculation, Q is therefore evaluated by nonlinear iteration procedure analogous to that employed in obtaining the circulation term Γ for an analysis problem. If there is trailing edge openness, and if the source term is not included in the far field, then the solution obtained may be questionable.

Wind Tunnel

To establish the appropriate boundary conditions on a finite computational domain for a tunnel simulation, the far field corresponding to $x \to \pm\infty$ has been derived using a Green's function method. Only the final results to the dominant order for the solid, ideal slotted and free jet tunnel wall cases are reported here. The airfoil is positioned midway between the walls. Thus, the airfoil slit is at $\tilde{y} = 0$ and the tunnel boundaries are at $\tilde{y} = \pm H$. The appropriate boundary conditions on the tunnel walls are

$$\begin{aligned} &\phi_{\tilde{y}}\,(x,\pm H) = 0 && \text{for solid wall} \\ &\phi_{\tilde{y}}\,(x,\pm H) \pm \frac{1}{FH}\,\phi(x,\pm H) = 0 && \text{for slotted and free jet} \end{aligned} \tag{8}$$

where F is the slot parameter:

$$F = \frac{s}{\pi H}\, \ell n\, \operatorname{cosec}\left(\frac{-a}{2s}\right) \tag{9}$$

where s is the distance between slot centers and a is the slot width. For free jet case $F = 0$.

To dominant order in the Karman-Guderley $(x,\tilde{y})$ plane, the far fields corresponding to these tunnel cases at $x \to \pm\infty$ are:

Solid wall:

$$4h\phi = \pm K^{-1/2}\left\{t(1)(x-1) + \int_{-1}^{1} t(\xi)\,d\xi\right\}$$

$$+ \frac{\gamma+1}{2K}\int_{-h}^{h} d\eta \int_{-\infty}^{\infty}\left[u^2(\xi,\eta) - \frac{[t(1)]^2}{16h^2}\right]d\xi + 2h\Gamma(\operatorname{sgn}\tilde{y})H(x) + O\left(e^{-\lambda_1|x|}\right) \tag{10}$$

where $t(1) = F_u(1) - F_\ell(1)$, ξ, η are dummy variables for x and y, $h = \sqrt{K}\, H$, $H(x) = 1$ for $x > 0$ and $H(x) = 0$ for $x < 0$, and $u = \phi_x$.

Slotted and free-jet wall:

$$\phi \to 0 \qquad \text{as } x \to -\infty$$

$$\phi \to \frac{\Gamma}{2} \operatorname{sgn} \tilde{y} - \frac{1}{1+\bar{\tau}} \frac{\tilde{y}}{H} + \cdots \quad \text{as } x \to +\infty \tag{11}$$

Eqs. (11) assume no downwash at upstream infinity. Other expressions can be derived for different upstream assumptions. In this connection, the drag, lift, and pressure distribution can be shown to be unaffected by addition of upstream down flow.

CONSISTENCY

When the pressure distribution from the analysis calculation is used as an input for design, a consistent discretization procedure would recover the airfoil shape exactly, even across the shock. To achieve this agreement, dummy points below the airfoil surface are used. Figure 4 shows the grid points near the airfoil surface. The points (i, j-1) are the dummy points.

Analysis

From the known airfoil shape $(\phi_{\tilde{y}})_{i,j}$, at the beginning of each relaxation cycle the dummy point values $\phi_{i,j-1}$ are obtained from the central difference formula

$$\phi_{i,j-1} = \phi_{i,j+1} - 2\Delta\tilde{y}(\phi_{\tilde{y}})_{i,j} \tag{12}$$

This expression is then used in the finite differenced form of $\phi_{\tilde{y}\tilde{y}}$ in Eq. (1) at the airfoil points (i,j)

$$\left[\left(K - (\gamma+1)\phi_x\right)\phi_{xx}\right]_{i,j} + \frac{2\phi_{i,j+1} - 2\phi_{i,j}}{(\Delta\tilde{y})^2}_{i,j} = \frac{2(\phi_{\tilde{y}})_{i,j}}{\Delta\tilde{y}} \tag{13}$$

The nonlinear term in Eq. (13) is central differenced at elliptic points and one-sided backward differenced at hyperbolic points. To improve stability near the sonic region Jameson's[8] pseudo-time operator is used in the relaxation procedure. Once the analysis procedure converges, the pressure distribution on the airfoil is computed at half node points

$$C_p\big|_{i-1/2,j} = -\frac{2\delta^{2/3}}{M_\infty^{3/4}}\,\phi_x\big|_{i-1/2,j} \tag{14}$$

where

$$\phi_x\big|_{i-1/2,j} = (\phi_{i,j} - \phi_{i-1,j})/(x_{i,j} - x_{i-1,j}) \tag{15}$$

Design

As mentioned earlier in this paper, a portion of the airfoil shape ($\phi_{\tilde{y}}$) near the nose is specified (from x = -1 to x = XD in Figure 2). On the portion of the airfoil under design, the pressure coefficient $C_{p_{i-1/2,j}}$ is specified at half node points. From $C_{p_{i-1/2,j}}$, the perturbation potential $\phi_{i,j}$ on the airfoil surface is obtained from Eqs. (14) and (15)

$$\phi_{i,j} = \phi_{i-1,j} - \frac{M_\infty^{3/4}}{2\delta^{2/3}}\,C_{p_{i-1/2,j}}(x_{i,j} - x_{i-1,j}) \tag{16}$$

At the airfoil grid points where the shape $\phi_{\tilde{y}}$ is specified, Eq. (13) is used to evaluate the potential $\phi_{i,j}$ (usual SLOR scheme). Since this potential keeps changing during the relaxation cycle, the potential $\phi_{i,j}$ over the designed portion is updated accordingly at the beginning of each relaxation cycle using Eq. (16). After the mixed analysis-design solution converges, the slope $(\phi_{\tilde{y}})_{i,j}$ of the resulting airfoil is computed from Eq. (13) as

$$\phi_{\tilde{y}}\big|_{i,j} = \frac{\Delta\tilde{y}}{2}\left[\left(K - (\gamma+1)\phi_x\right)\phi_{xx}\right]_{i,j} + \frac{1}{\Delta\tilde{y}}\,(\phi_{i,j+1} - \phi_{i,j}) \tag{17}$$

From the slope $\phi_{\tilde{y}}$, the airfoil ordinates are calculated from the quadrature formula

$$y_{u,\ell}(x) = y_{u,\ell}(x_D) + \delta \int_{x_D}^{x} \left\{ \phi_{\tilde{y}} \Big|_{u,\ell} + \frac{\alpha}{\delta} \right\} dx \qquad (18)$$

$$x_D \leq x \leq 1$$

where $y_{u,\ell}(XD)$ are the upper and lower y values of the airfoil at X = XD, where the boundary condition changes from analysis to design. Since Eqs. (13), (14), and (15) are used in the same manner in the analysis and design, the discretization procedure is consistent.

RESULTS

To check the consistency logic developed in the previous section, a test case was run. An analysis calculation for the NACA 0012 airfoil at $M_\infty = 0.75$, $\alpha = 2°$ was first performed. The pressure distribution from the analysis calculation was then used as an input for the design problem to check if the NACA 0012 airfoil shape would be recovered even across the shock. The results are shown in Table 1. The upper (y_u) and lower (y_ℓ) surface ordinates from the design calculation agreed with the original NACA 0012 airfoil up to four significant figures, thus establishing consistency of the method.

Figure 5 shows a design calculation performed on the previous NACA 0012 analysis solution to get rid of the upper surface shock. The dotted line shows the analysis solution, and the solid line shows the prescribed shockless pressure distribution. The resulting airfoil is shown by the solid line. It is seen that a slight flattening of the upper surface determined in the design phase eliminates the shock. This reshaping produces an openness at the trailing edge which was properly accounted for by the effective source term in the far field.

Analysis calculations were performed over the shock-free airfoil designed in free air, (shown in Figure 5), using solid wall tunnel boundary conditions. The airfoil that produces a shockless pressure distribution in free air may produce a shock when tested in the wind tunnel. This is illustrated by the results shown in Figure 6. From the figure, it is evident that when the tunnel wall is sufficiently far away from the airfoil, the pressure distribution remains shockless. As the tunnel wall is brought closer to the airfoil, the shock appears and moves downstream.

Figure 7 shows a supercritical airfoil design with NACA 0012 nose shape. First, an analysis solution was generated over the NACA 0012 airfoil at $M_\infty = 0.8$ and $\alpha = 2°$. This is shown by the dotted line in Figure 7. Then a supercritical pressure distribution was specified with a large loading on the aft end of the airfoil. The resulting airfoil resembles a Whitcomb type supercritical airfoil which is characterized by a substantially reduced curvature on the mid chord region of the upper surface together with increased camber near the trailing edge.

An off design calculation of this supercritical airfoil at $M_\infty = 0.78$ is shown in Figure 8. For qualitative comparison, off design and design calculations on the NASA 11% thick supercritical airfoil are also shown. At off design Mach numbers the shock reappears.

The effect of wind tunnel walls on the performance of the free air shock free supercritical airfoil is shown in Figure 9. Only the upper surface pressure is shown for solid, ideal slotted ($F = 0.279$) and free jet ($F = 0$) tunnel cases. The solid line in Figure 9 refers to the shock free, free air pressure distribution. For tunnel wall height to a chord ratio of 6, the shock reappears in all the tunnel wall cases. As expected, the solid wall produces a stronger shock while the free jet case produces a weaker one.

CONCLUDING REMARKS

An efficient and inexpensive design-analysis code has been developed for two-dimensional airfoils. The consistent differencing procedure employed at the airfoil boundary allows use of the same code in either analysis or design-analysis mode without requiring any modification. In the algorithm, the effect of an open trailing edge is properly accounted for, a factor ignored by other workers. The fact that no mapping is involved in the two-dimensional work makes the extension of the algorithm to three dimensional wing design feasible and attractive.

REFERENCES

1. Nieuwland, G. Y., "Transonic Potential Flow Around a Family of Quasi-Elliptical Aerofoil Sections," NLR-TR-T.172, National Lucht-en Ruimtevaart Laboratorium, Amsterdam, 1967.
2. Garabedian, P. R., and Korn, D. G., "Numerical Design of Transonic Airfoils," Numerical Solution of Partial Differential Equations--II, Academic Press, 1971.
3. Steger, J. L., and Klineberg, J. M., "A Finite Difference Method for Transonic Airfoil Design," AIAA J., Vol. 11, No. 5, May 1973, pp. 628-635.
4. Tranen, T. L., "A Rapid Computer Aided Transonic Airfoil Design Method," AIAA Paper No. 74-501, June 1974.
5. Carlson, L. A., "Transonic Airfoil Analysis and Design Using Cartesian Coordinates," Proc. AIAA 2nd Computational Fluid Dynamics Conference, June 19-20, 1975, pp. 175-183.
6. Whitcomb, R. T., "Review of NASA Supercritical Airfoils," ICAS Paper 74-10, August 1974.
7. Cole, J. D., "Twenty Years of Transonic Flow," Document G1-82-0878, July 1969, Boeing Scientific Research Laboratories, Seattle, Wash.
8. Jameson, A., "Iterative Solutions of Transonic Flows over Airfoils and Wings, Including Flows at Mach 1," Communications of Pure and Applied Mathematics, Vol. 27, 1974, pp. 283-309.

TABLE 1.- CONSISTENCY CHECK

$[M_\infty = 0.75;\ \alpha = 2^0]$

x/C	y Analysis		C_p		y Design	
	Upper	Lower	Upper	Lower	Upper	Lower
.045	3.47139	-3.4713	-.73743	.24451	3.47139	-3.47139
.075	4.27675	-4.2767	-.88529	-.00489	4.27675	-4.27675
.265625	6.05798	-6.0579	-1.1407	-.3006	6.05801	-6.05799
.39	5.92235	-5.9223	-1.1547	-.26837	5.92242	-5.92238
.453125	5.65088	-5.6508	-.46496	-.23615	5.65097	-5.65091
.546875	5.06204	-5.0620	-.37826	-.18103	5.06215	-5.06207
.765625	3.08328	-3.0832	-.14389	-.03554	3.08347	-3.08335
.96	.76099	-.7609	.18687	.22115	.76102	-0.76101

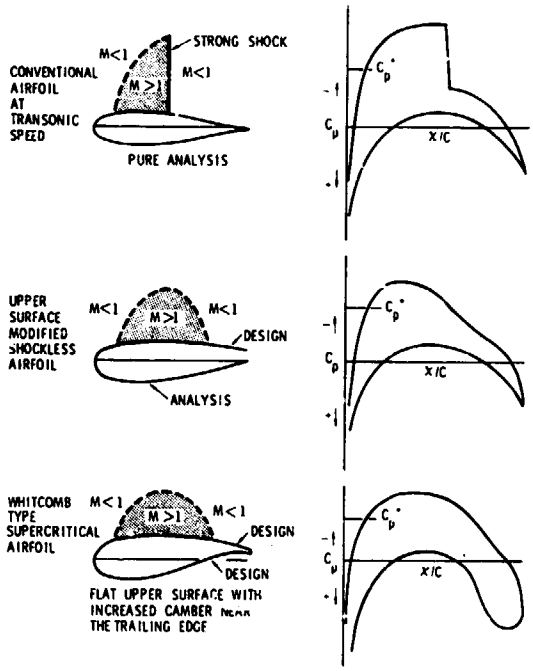

Figure 1.- Supercritical airfoil design.

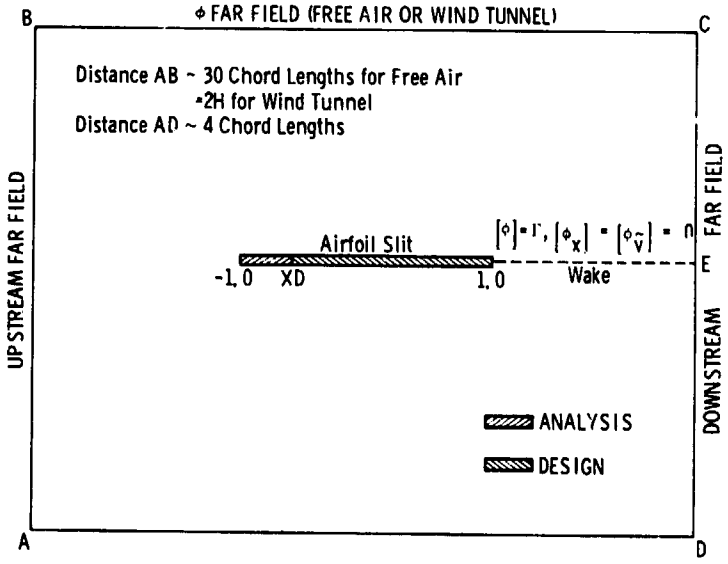

Figure 2.- Boundary conditions and far-field arrangement.

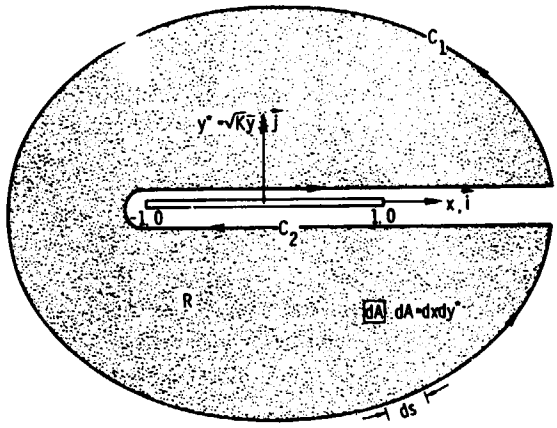

$$\int_{-1}^{1} |\phi_{\tilde{y}}| dx = \oint_{C_1} \left(K\phi_x - \frac{\gamma+1}{2}\phi_x^2\right) d\tilde{y} - \phi_{\tilde{y}} dx$$

$$Q = \frac{1}{\sqrt{K}} \int_{-1}^{1} |\phi_{\tilde{y}}| dx$$

Figure 3.- Cut region for far field.

$$\phi_{\tilde{y}}\Big|_{i,j} = \frac{\phi_{i,j+1} - \phi_{i,j-1}}{2\Delta\tilde{y}}$$

$$\phi_x\Big|_{i-1/2,j} = \frac{\phi_{i,j} - \phi_{i-1,j}}{\Delta x}$$

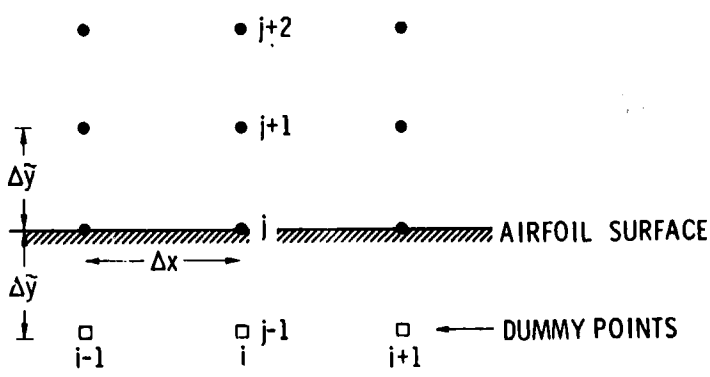

Figure 4.- Dummy-point arrangement.

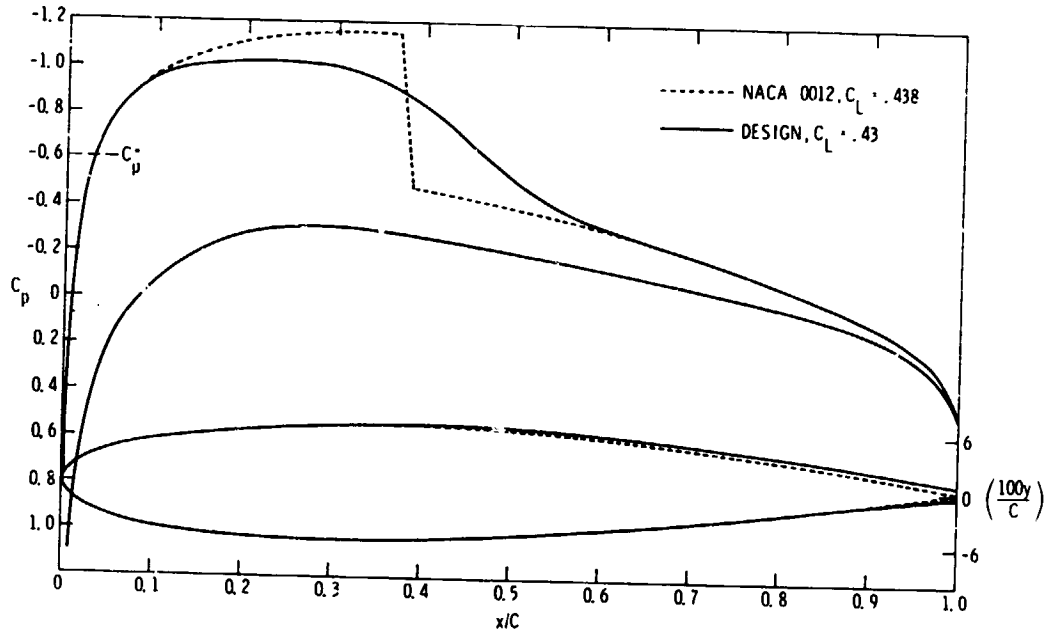

Figure 5.- Transonic design. Shock elimination. $\alpha = 2°$; $M_\infty = 0.75$.

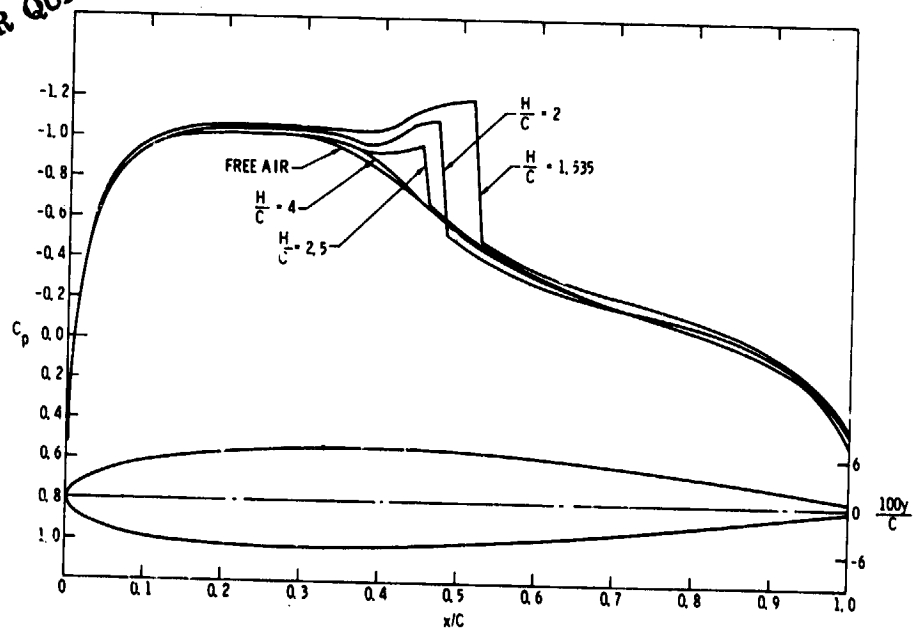

Figure 6.- Effect of solid tunnel walls on the performance of a free-flight shock-free airfoil. $M_\infty = 0.75$; $\alpha = 2°$.

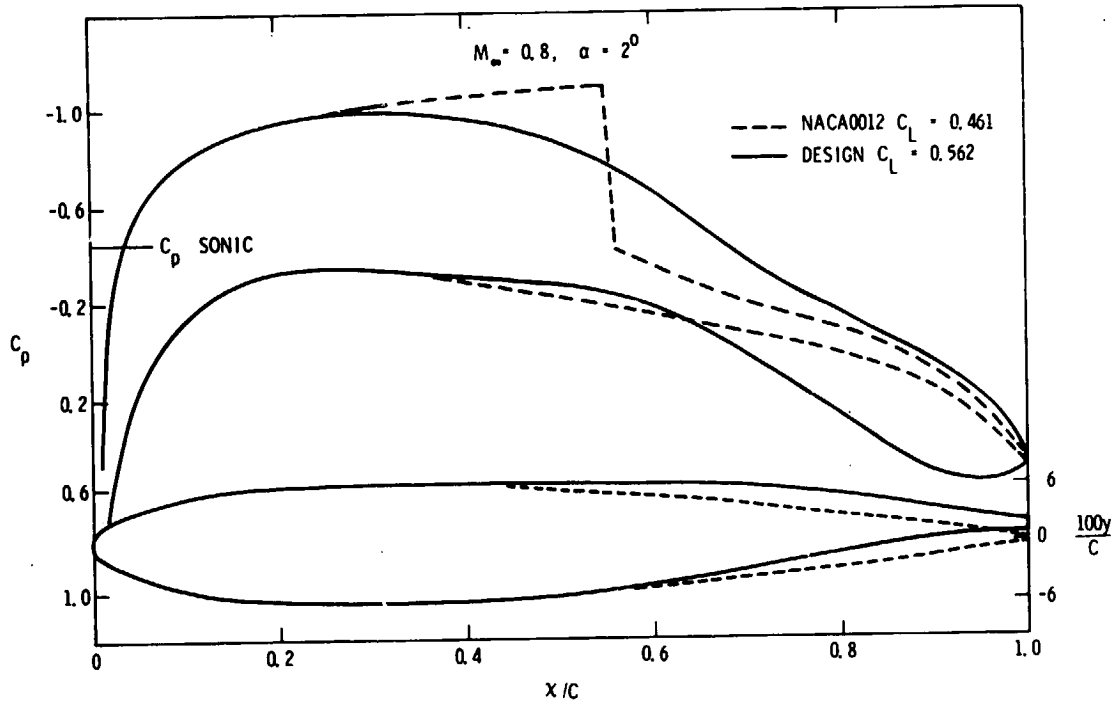

Figure 7.- Supercritical-airfoil design with NACA 0012 nose shape. $M_\infty = 0.8$; $\alpha = 2°$.

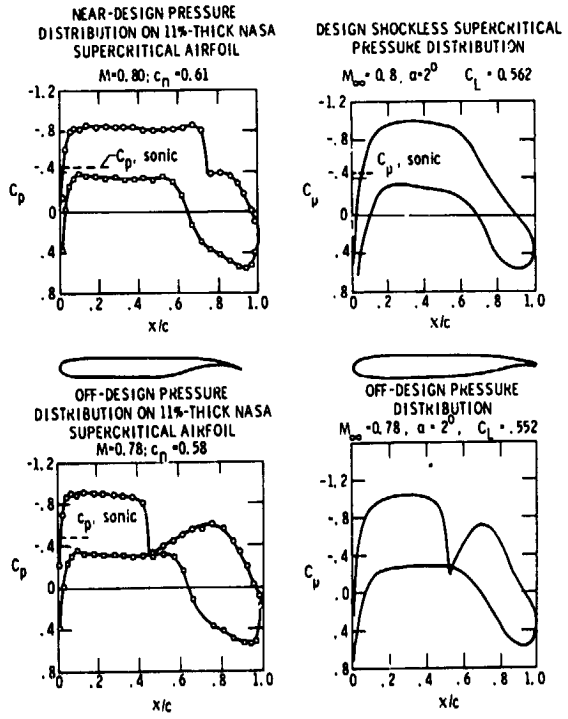

Figure 8.- Off-design pressure distribution.

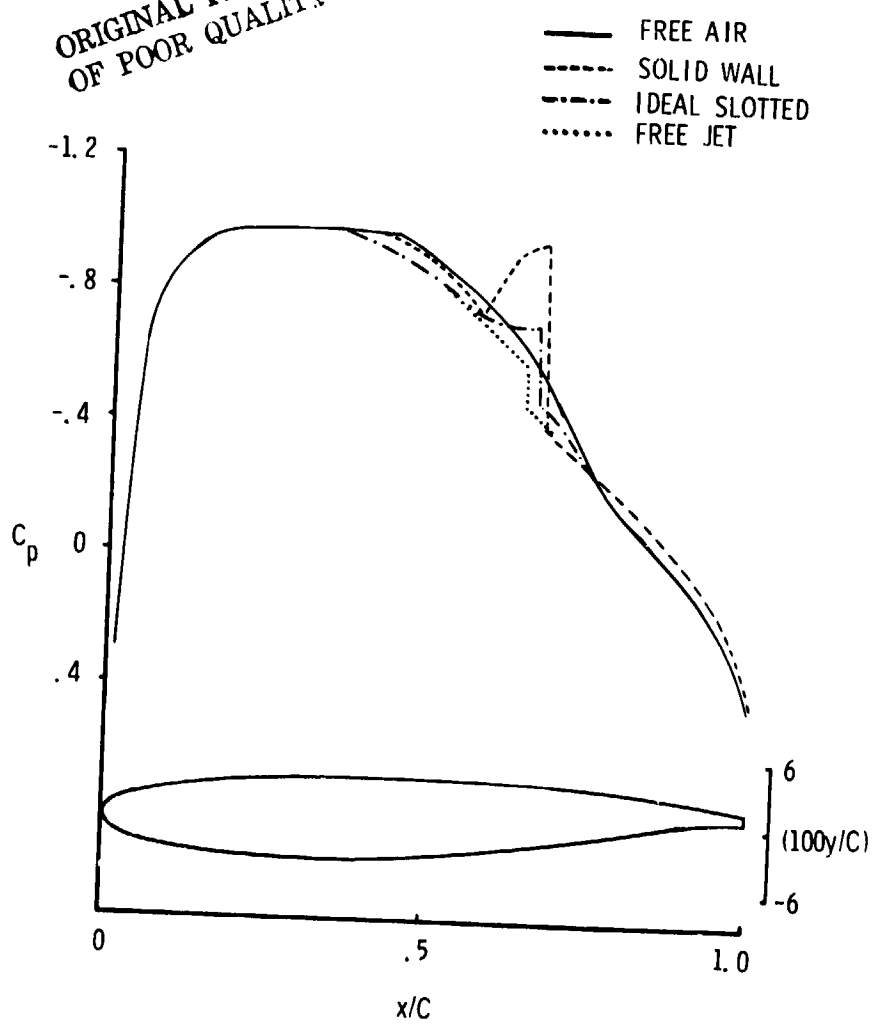

Figure 9.- Performance of a free-flight shock-free airfoil in a wind tunnel. $M_\infty = 0.8$; $\alpha = 2°$; $H/C = 6$.